JOURNAL OF AIRCRAFT
Vol. 47, No. 6, November–December 2010

Engineering Notes

Flow-Separation Lines on Axisymmetric Bodies with Tapered Tails

T. L. Jeans*
Defence Research and Development Canada—Atlantic, Dartmouth, Nova Scotia, B2Y 3Z7, Canada
and
A. G. L. Holloway†
University of New Brunswick, Fredericton, New Brunswick E3A 6S3, Canada

DOI: 10.2514/1.C031141

Nomenclature

a	=	local body radius
$a_{\max}$	=	maximum body radius
a^*	=	dimensionless body radius, $a/a_{\max}$
$\lvert C_f \rvert$	=	skin-friction magnitude, $\lvert \boldsymbol{\tau}_w \rvert / q$
C_{pc}	=	crossflow pressure coefficient, $(p - p_\infty)/q\sin^2\alpha$
H	=	Heaviside unit step function
l	=	body length
p	=	pressure
q	=	freestream dynamic pressure, $(\rho U^2)/2$
Re	=	Reynolds number based on body length, $(\rho U l)/\mu$
t	=	time
t^*	=	dimensionless time, $(tv)/a$
U	=	freestream velocity magnitude
u, v	=	longitudinal and lateral freestream velocity components
α	=	angle of incidence
θ	=	angular position of separation point measured from the windward side
θ_o	=	initial angle of separation
θ_∞	=	equilibrium angle of separation
θ^*	=	normalized separation point, $(\theta - \theta_\infty)/(\theta_o - \theta_\infty)$
λ	=	longitudinal distance aft from the nose
μ	=	dynamic viscosity
ρ	=	fluid density

I. Introduction

WHEN a slender body of revolution translates at moderate incidence ($5\,\text{deg} \leq \alpha \leq 30\,\text{deg}$), adverse pressure gradients due to the crossflow cause the boundary layer to separate on the leeside and produce two shear layers that roll up to form symmetric vortices of opposite rotation [1,2]. The flow separation results in significant aerodynamic forces and moments that depend strongly on incidence. Although these bodies have relatively simple geometry, they have been historically difficult to model, because they lack sharp edges that fix the separation lines. The present work extends the separation-line model of Schindel [3], developed for missiles, to bodies of varying cross-sectional area, allowing one to predict the separation line along the tapered tail.

The qualitative nature of separation around three-dimensional bodies immersed in a flow and its relationship to lines of skin friction and the surface vorticity has been described by Lighthill [4]. Separation on slender bodies of revolution, in particular, has been extensively investigated [5–11]. Yates and Chapman [5] qualitatively examined the related separation kinematics and characterized the topology as open, because the resulting separation line has a free endpoint on the surface. They concluded that crossflow separation does not originate from a unique singularity on the body surface, as is the case for many types of separation. Instead, all surface streamlines originate from the stagnation point on the nose. Simpson [6] investigated the qualitative traits of crossflow separation on slender bodies of revolution and concluded that the most important side effect of separation, and thus its defining trait, is the breakdown of the normal boundary-layer flow, resulting in a significant departure of fluid away from the body surface. Since no fluid can pass through this departed sheet of fluid, streamlines on either side of a separation converge asymptotically toward the separation line. Wetzel and Simpson [7] extended this work and developed methods for quantitatively identifying separation lines on a prolate spheroid. They compared several measurement techniques for determining the separation location (including converging skin-friction lines, maximum normal wall-normal velocity, skin-friction magnitude minima, and changes in surface pressure) and concluded, for practical purposes, that flow separation from axisymmetric bodies at moderate incidence is located near minimums in wall shear stress magnitude in each cross-sectional plane [7]. This is the method that will be used directly in the following to locate the primary separation lines from computational data. For experimental studies to which we refer, a combination of oil streaklines on the surface and surface heat transfer rates have been used to infer the location of separation lines.

II. Model Geometries

The database used for the current study included four slender bodies of revolution all having a round nose and tapered tail. In particular these were: the Defence Research and Development Canada (DRDC) Static-Test-Rig (STR) hullform [12], the Defence Advanced Research Projects Agency (DARPA) SUBOFF model 5470 hullform [13], the U.S. Naval Surface Warfare Center Carderock Division Series-58 Model 4621 hullform [14], and the 6:1 spheroid. These bodies were chosen primarily because experimental measurements and/or computational predictions of separation lines as a function of incidence existed in the open literature. Profiles of each geometry are shown in Fig. 1, with the body radius and longitudinal distance from the nose normalized by body length.

III. Experimental and Computational Database

A. Experimental Database

All of the profiles shown in Fig. 1 have been previously studied experimentally; however, flow visualization and/or measurements of the separation location are only available for the DRDC STR and 6:1 spheroid geometries.

1. DRDC STR

In 1988, wind-tunnel tests were performed on the DRDC STR geometry in a 9 m wind tunnel at the National Research Council of Canada Institute for Aerospace Research at Reynolds numbers up to 23×10^6 and incidence up to 30 [12]. A 1/10th-scale model was

Received 14 June 2010; revision received 1 September 2010; accepted for publication 2 September 2010.

*Defence Scientist, Warship Performance, 9 Grove Street, P.O. Box 1012
†Professor, Department of Mechanical Engineering, 15 Dineen Drive. P.O. Box 4400.

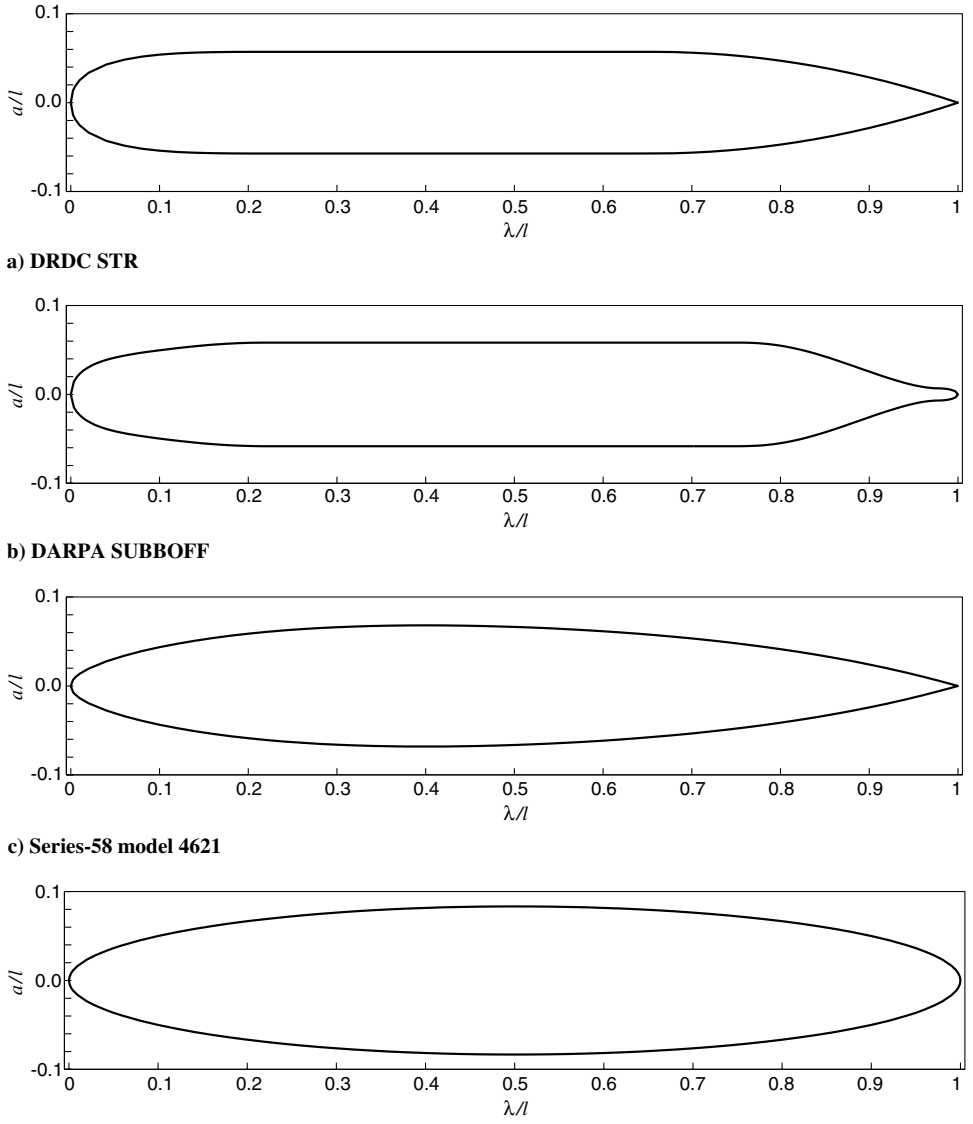

Fig. 1 Profiles of the slender bodies of revolution investigated.

used and turbulent boundary-layer transition trips were located 3% of the hull length from the nose for all tests. For a limited number of tests skin-friction lines were made visible by applying an oil and titanium dioxide mixture to the surface of the body. Lines of convergence indicate regions of boundary-layer separation and lines of divergence indicate reattachment regions. Experimental skin-friction lines at $Re = 23 \times 10^6$ and $\alpha = 20$ deg are shown in Fig. 2a and an estimate of the primary separation-line location based on visual inspection of

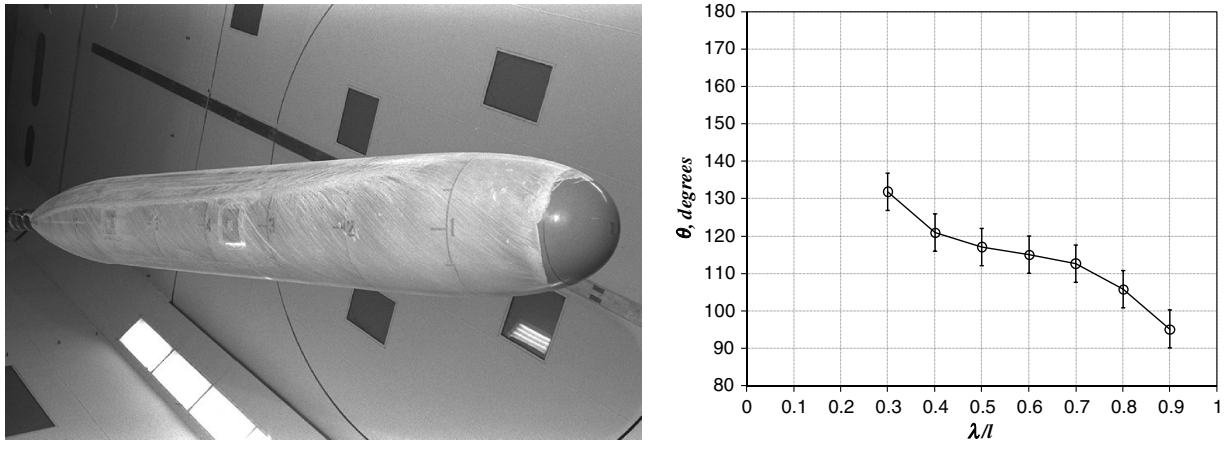

Fig. 2 DRDC STR hull at $Re = 23 \times 10^6$ and $\alpha = 20$ deg: a) oil surface streaklines and b) estimate of the separation-line location based on visual inspection of the oil streaks.

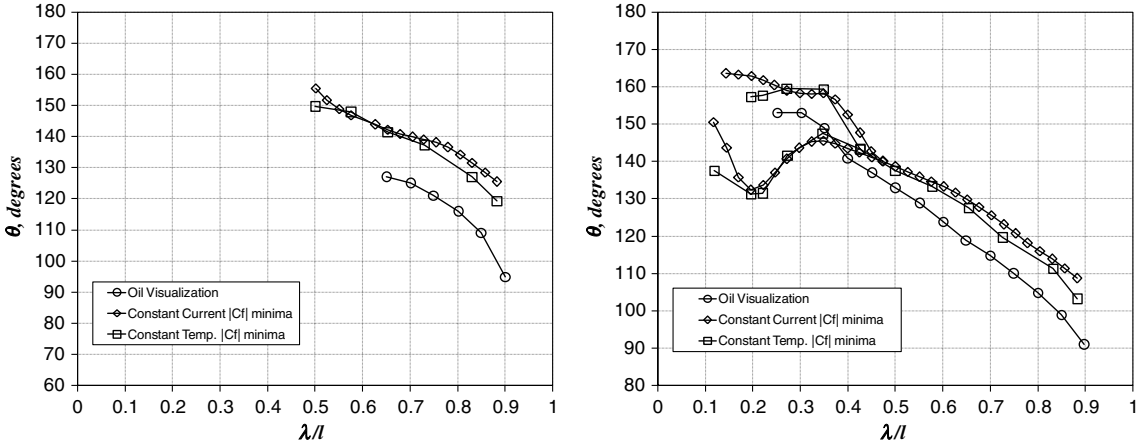

a) $\alpha = 10^o$ b) $\alpha = 20^o$

Fig. 3 Separation lines measured on a 6:1 spheroid at $Re = 4.2 \times 10^6$ using oil visualization and skin-friction magnitude minima. Reproduced from [7].

the oil streaks is shown in Fig. 2b. The uncertainty of the visual inspection procedure was estimated to be $\delta_\theta = \pm 5$ deg.

2. 6:1 Spheroid

Between 1992 and 1998, Ahn and Simpson [8], Chesnakas and Simpson [9], and Wetzel and Simpson [7] completed wind-tunnel tests on a 6:1 ellipsoid at the Virginia Polytechnic Institute and State University at Reynolds numbers up to 4.2×10^6 and incident angles up to 30 deg. For all studies turbulent boundary-layer transition trips were located 20% of the hull length from the nose. Skin-friction lines were made visible by applying an oil-based mixture to the body surface, laser Doppler velocimetry was used to accurately measure near-wall velocity components, and surface-mounted hot-film sensors were used to estimate local skin friction. A subset of their results showing separation lines based on oil visualization and skin-friction magnitude minima are reproduced in Fig. 3. In general, oil visualization indicates separation windward of the skin-friction minima by approximately 10–15 deg at both $\alpha = 10$ and 20 deg.

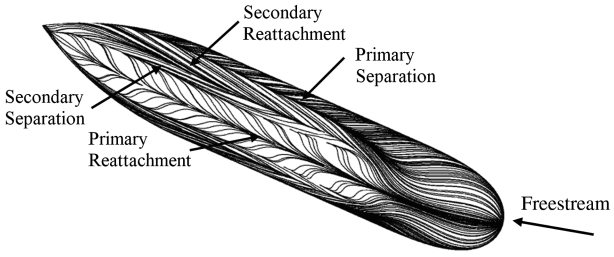

Fig. 4 RANS predictions of surface shear stress lines for the DRDC STR geometry at $Re = 23 \times 10^6$ and $\alpha = 30$ deg.

B. Computational Database

The computational fluid dynamics (CFD) database consists of predictions from verified and validated Reynolds-averaged Navier–Stokes (RANS) simulations on the DRDC STR, Series-58 Model 4621, and DARPA SUBOFF geometries using ANSYS CFX, a commercially available solver (see [10,11] for details). The primary means of validation was comparison of overall forces and moments with experiment [12,14–17], as presented in detail in [10]. The RANS simulations were found to be within experimental uncertainty for the DRDC STR geometry for $\alpha < 25$ deg. Simulations were completed at model scale, and incidence angles up to 30 deg using a scripted hybrid meshing algorithm that adapted the structured grid to the wake (see [18–20] for details). Several turbulence models were investigated and the best agreement with experimental data was obtained with the Reynolds stress model [21].

The CFD predictions provide a high level of flow detail that is difficult to obtain from experiment. This includes complete surface pressure and skin-friction distributions. The topology of the leeside skin-friction lines for the DRDC STR geometry at $Re = 23 \times 10^6$ and $\alpha = 30$ deg from the RANS predictions is shown in Fig. 4. Regions of primary and secondary separation and reattachment are identified by convergence and divergence of skin-friction lines. The

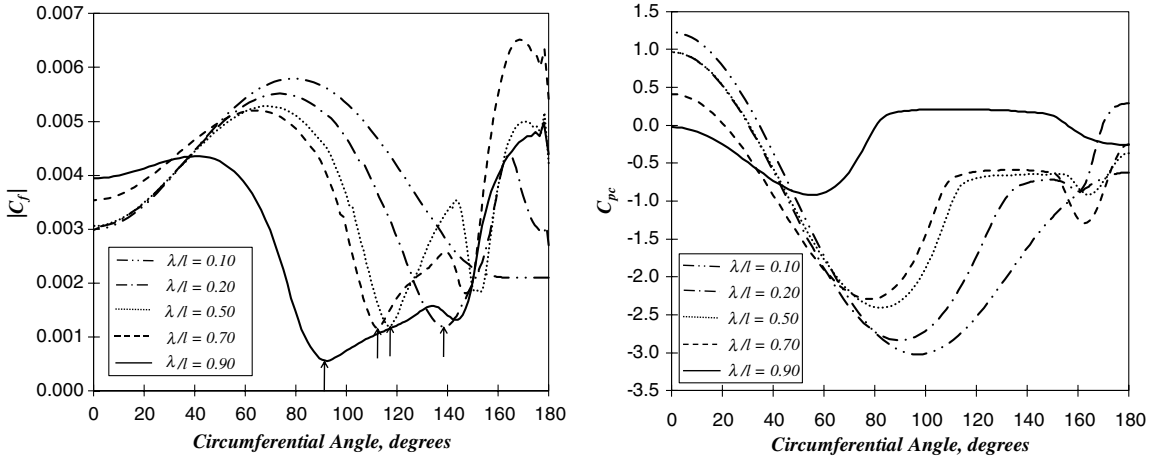

a) Skin friction b) Surface pressure

Fig. 5 RANS predictions of circumferential variation of surface pressure and skin-friction magnitude at constant axial locations for the DRDC STR geometry at $Re = 23 \times 10^6$ and $\alpha = 30$ deg. Arrows indicate the minima used to locate the primary separation line.

topology of the skin-friction lines are visibly similar to those previously shown in Fig. 2a.

Corresponding circumferential skin-friction distributions at constant axial locations are plotted in Fig. 5a, where $|C_f|$ is the magnitude of wall shear stress, normalized by the freestream dynamic pressure. These distributions allow one to accurately determine the circumferential location of local minima in skin friction. At $\lambda/l = 0.10$, $|C_f|$ has no minimum; therefore, it is inferred the flow remains attached in this region. At $\lambda/l = 0.20$, a local minimum is visible at $\theta = 139$ deg, indicating the flow has separated. A primary minimum that continually migrates windward is evident in all the remaining $|C_f|$ distributions. For all the distributions where $\lambda/l >$ 0.20, a secondary minimum occurs between $\theta = 145$–150 deg, indicating a secondary separation.

Circumferential surface pressure distributions are plotted in Fig. 5b, with the crossflow pressure coefficient C_{pc} normalized using the crossflow speed $U\sin(\alpha)$ (making values greater than 1 possible). Most notable is that for each distribution the maximum suction (minimum C_{pc}) continually diminishes and migrates windward as the flow progresses along the body.

Using the criterion of Wetzel and Simpson [7], skin-friction magnitude minima of the RANS predictions were used to determine primary flow-separation lines. Results are plotted in Fig. 6 for the DRDC STR geometry at $Re = 23 \times 10^6$ and $\alpha = 10$ deg, 15, 20, 25 and 30 deg, the Series-58 Model 4621 geometry at $Re = 11.7 \times 10^6$ and $\alpha = 6$ deg, 12, and 18 deg, and the DARPA SUBOFF geometry at $Re = 14 \times 10^6$ and $\alpha = 8$ deg and 12 deg. The uncertainty in the local skin-friction minimum is $\delta_\theta = \pm 1$ deg based on the resolution of the computational grid. It is clear in Fig. 6 that the primary separation is body profile-dependent, and that, at a given axial position, separation occurs earlier as incidence is increased. Once the flow has separated, the separation line migrates continuously windward with the rate of migration increasing along the tapered tail.

To show the relationship between the line of primary flow separation and the line of minimum pressure, the latter is also plotted in Fig. 6a based on RANS predictions of the DRDC STR geometry at $Re = 23 \times 10^6$ and $\alpha = 30$ deg. The minimum-pressure line has the same general trend as the line of separation, but is windward of the separation point at all axial positions. Initially, the point of minimum pressure is approximately 55 deg windward of the separation point, with this difference decreasing to approximately 37 deg by $\lambda/l = 0.35$, which is similar to observations for a supercritical flow over a cylinder. Along the remainder of the body the difference between the separation and minimum-pressure lines remains relatively constant with values between 37 and 32 deg.

IV. Separation-Line Model

The present separation-line model is based on an analogy between transient crossflow over two-dimensional circular cylinders and separated flow over slender bodies of revolution at incidence (see [22]). This analogy transforms time t for the transient problem to axial position λ along the body of revolution at incidence according to

$$t = \frac{\lambda}{U\cos(\alpha)} \tag{1}$$

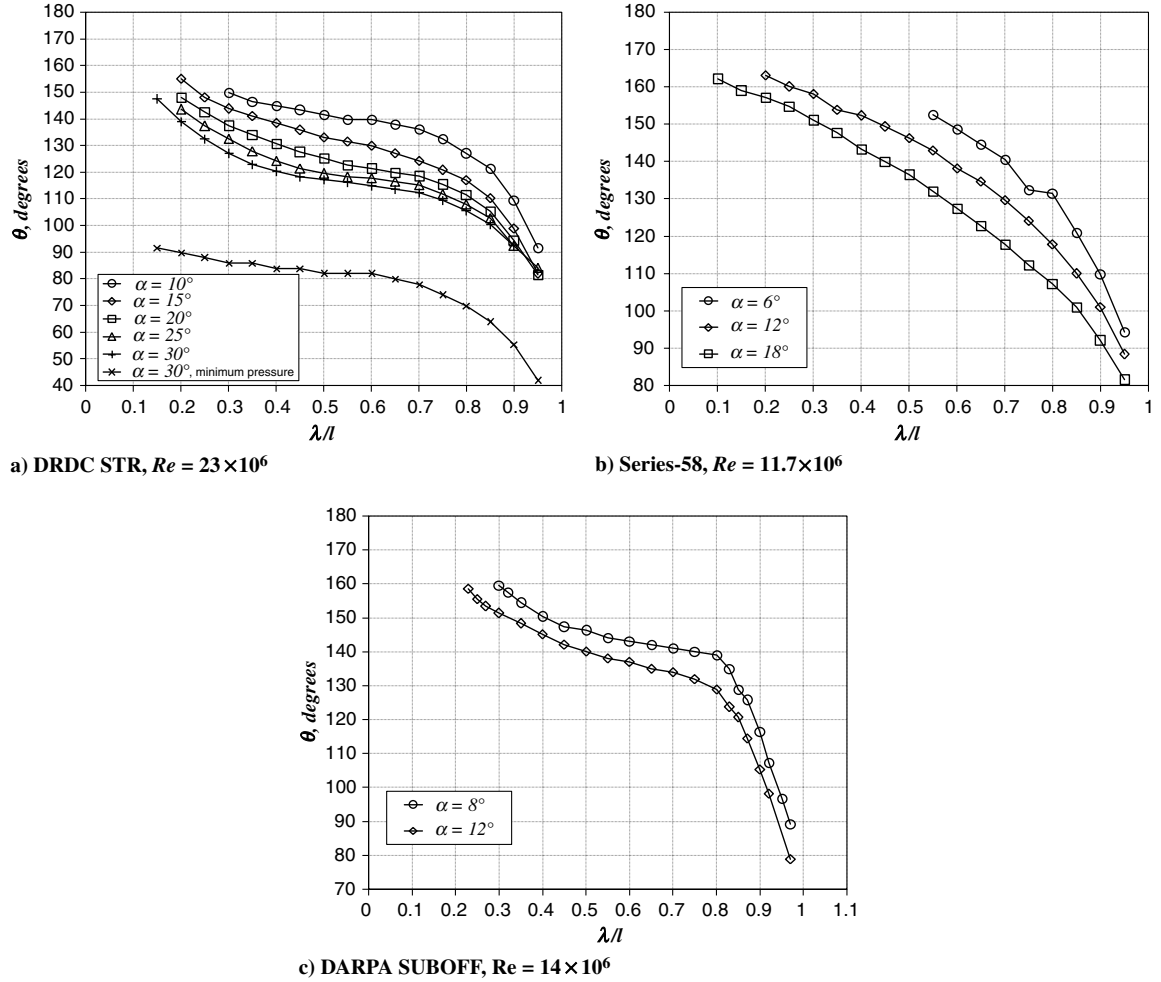

a) DRDC STR, $Re = 23 \times 10^6$

b) Series-58, $Re = 11.7 \times 10^6$

c) DARPA SUBOFF, Re = 14×10^6

Fig. 6 RANS predictions of primary separation lines for the DRDC STR, Series-58, and DARPA SUBOFF geometries. These results are based on skin-friction magnitude minima.

or in dimensionless form as

$$t^* = \frac{tv}{a} = \frac{\lambda}{a}\tan(\alpha) \tag{2}$$

where $U\cos(\alpha)$ is the longitudinal component of the freestream velocity, $v = U\sin(\alpha)$ is the crossflow velocity, and a is body radius [23]. Schindel [3] noted that for two-dimensional impulsively started cylinders the separation angle exponentially approached its equilibrium value in time, and based on this observation, together with the above analogy, he developed an expression for the separation line along slender bodies with a conical nose and constant-diameter midbody (i.e., missile-shaped bodies).

Here, we extend Schindel's [3] model for slender bodies of revolution with tapered tails by including the effect of a varying-body radius. Noting that along the tapered tail the separation line moves windward in concert with the minimum-pressure location, which depends on $\mathrm{d}a/\mathrm{d}x$, we propose that the separation line can be modeled according to

$$\frac{\mathrm{d}\theta^*}{\mathrm{d}t^*} + \kappa_h\theta^* = \kappa_p\frac{\mathrm{d}a^*}{\mathrm{d}t^*}H(t^* - t^*_{\mathrm{sep}}) \tag{3}$$

where θ^* is the dimensionless separation angle defined as $\theta^* = (\theta - \theta_\infty)/(\theta_o - \theta_\infty)$, θ_∞ is the steady-state separation angle, and θ_o is arbitrarily chosen to be $\theta_o = 180\,\mathrm{deg}$. The unit function $H(t^* - t^*_{\mathrm{sep}})$ is zero for $t^* < t^*_{\mathrm{sep}}$ and unity for $t^* \geq t^*_{\mathrm{sep}}$, where t^*_{sep} corresponds to the first appearance of separation on the body. The left-hand-side of Eq. (3) is equivalent to the original model proposed by Schindel [3] and simply states that for a constant body radius the local separation angle approaches the steady-state value, θ_∞, at an exponential rate determined by the constant κ_h. This steady-state separation angle was taken equal to the separation angle for supercritical flow over cylinders. The profile-dependent term on the right-hand-side of Eq. (3), introduced by the present authors, is taken proportional to the rate of change of body radius as $\kappa_p\mathrm{d}a^*/\mathrm{d}t^*$, where in this context $a^* = a/a_{\max}$, $t^* = tv/a_{\max}$, and κ_p is an empirically determined constant. Note that the choice of $a_{\max}$ plays no direct role in the determination of θ, because $\mathrm{d}a^*/\mathrm{d}t^*$ reduces to $(\mathrm{d}a/\mathrm{d}x)\mathrm{cotan}(\alpha)$.

Integrating Eq. (3) from the first point at which separation is observed, t^*_{sep}, aft to any position $t^* > t^*_{\mathrm{sep}}$ gives

$$\theta^* = \theta^*_{\mathrm{sep}}e^{\kappa_h t^*_{\mathrm{sep}}}e^{-\kappa_h t^*} + e^{-\kappa_h t^*}\int_{t^*_{\mathrm{sep}}}^{t^*} e^{\kappa_h \tau^*}\kappa_p\frac{\mathrm{d}a^*}{\mathrm{d}\tau^*}\,\mathrm{d}\tau^* \tag{4}$$

It will be assumed as an additional hypothesis that $\theta^*_{\mathrm{sep}}e^{\kappa_h t^*_{\mathrm{sep}}} = 1$, which effectively requires that separation always originates along the exponential line extending from $\theta = 180\,\mathrm{deg}$ at $t^* = 0$ to $\theta = \theta_\infty$ at $t^* \to \infty$.

V. Results and Discussion

A. Fitting the Empirical Constants

To test the hypotheses proposed in Sec. IV, the separation lines in Figs. 6 are repeated in Fig. 7 with t^* as the abscissa. An important feature of this figure is the complete collapse of both the DRDC STR and DARPA SUBOFF data along the constant-diameter midbody region for all angles of incidence. For these geometries the flow does not separate until the constant-diameter midbody region is reached,

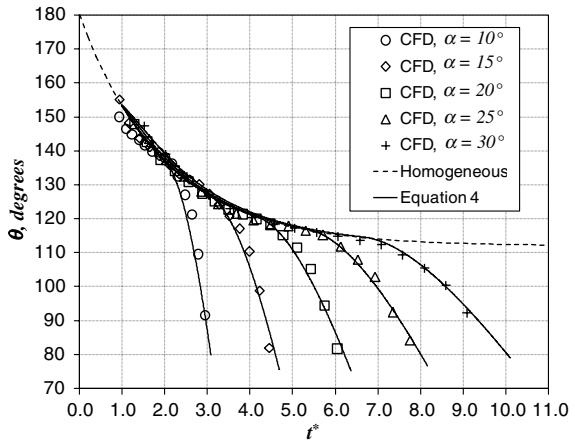

a) DRDC STR, $Re = 23\times10^6$

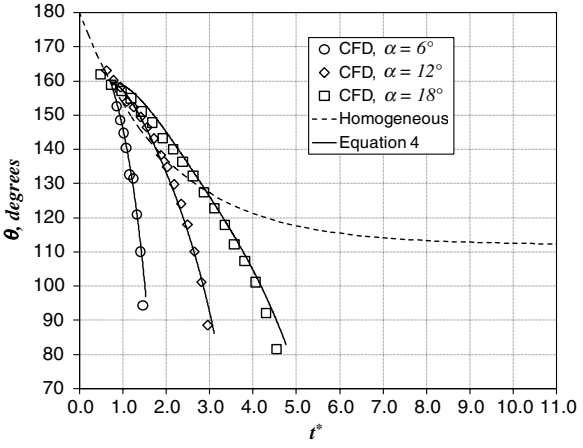

b) Series-58 model 4621, $Re = 11.7\times10^6$

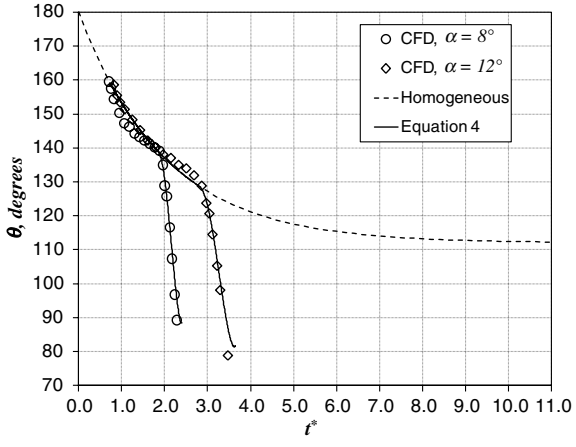

c) DARPA SUBOFF, Re = 14×10^6

Fig. 7 Comparison of modeled and RANS predicted lines of primary flow separation for the DRDC STR, Series-58, and DARPA SUBOFF hulls. The abscissa is dimensionless time measured in a frame moving at the longitudinal component of freestream velocity.

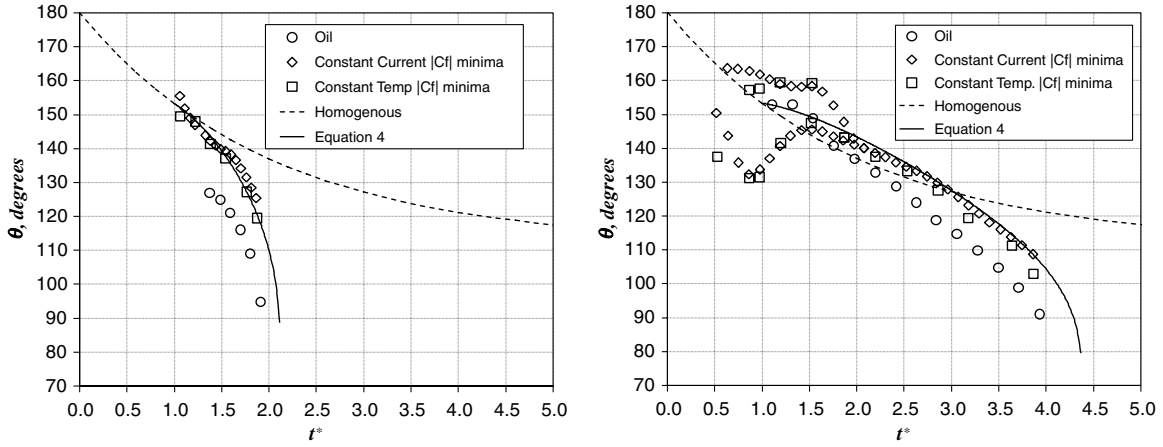

a) $\alpha = 10^o$ b) $\alpha = 20^o$

Fig. 8 Comparison of modeled and experimentally predicted lines of primary flow separation for the 6:1 spheroid at $Re = 4.2 \times 10^6$. The abscissa is dimensionless time measured in a frame moving at the longitudinal component of freestream velocity.

and a significant portion is therefore represented by the homogenous part of Eq. (4), as indicated by the dashed line. These data were used to empirically determine θ_∞ and κ_h, with the best fit achieved with $\theta_\infty = 112$ deg and $\kappa_h = 0.5$. Schindel [3] estimated that $\kappa_h = 0.7$, and according to Panton [24] the steady separation angle for supercritical two-dimensional flow over cylinders is $\theta_\infty = 115$ deg. Consistent with $\theta^*_{\text{sep}} e^{\kappa_h t^*_{\text{sep}}} = 1$, separation originates along the dashed line for $\alpha \geq 15$ deg.

The solution for θ^* along the tail was determined for each geometry by numerically integrating the particular component of Eq. (4) for each profile and adding it to the homogenous part, $e^{-\kappa_h t^*}$. Using the result from the DRDC STR data κ_p was empirically fitted as $\kappa_p = 0.809$, and this value was used for all other geometries.

B. Comparison of Model Predictions to Computational and Experimental Data

Separation lines predicted by Eq. (4) are shown for the DRDC STR, Series-58 Model 4621, DARPA SUBOFF, and 6:1 spheroid geometries in Figs. 7 and 8. For all geometries and at all incidence angles, the model predictions are in excellent agreement with the RANS and experimental data along the tapered tails. In addition, the model correctly predicts that along the nose of the Series-58 Model 4621 at $\alpha = 12$ and 18 deg, and the 6:1 spheroid data at $\alpha = 20$ deg the separation line is leeward of the dashed line due to the increasing body radius. These results are consistent with the underlying assumption of the model that the separation lines along the tail of axisymmetric slender bodies in translation at incidence are locally determined and primarily driven by $(\mathrm{d}a/\mathrm{d}x)\mathrm{cotan}(\alpha)$. Thus, the primary separation line is strongly dependent on the outer flow and its pressure field.

An exception to the agreement cited above is the constant temperature hot-film data for the 6:1 spheroid at $\alpha = 20$ deg and $t^* < 2.0$ that is shown in Fig. 8b. These data have the lowest Reynolds number of the study and possibly include transitional effects and are therefore more complex than the simple model presented in this Note will allow, but it is worth noting that the constant current hot-film data and oil data, allowing for a 10 deg offset, agree quantitatively with the model.

C. Dependence of Model Predictions on t^*_{sep}

The only empirical parameter of the model that was found to vary between data sets was t^*_{sep}. Physically, t^*_{sep} is the nondimensional axial distance from the nose where flow separation first occurs, which, as noted by Yates and Chapman [5], is very difficult to determine. In general, one would expect t^*_{sep} to depend on nose shape, Reynolds number (where $Re < 2.5 \times 10^6$)[8], wind-tunnel turbulence levels, trip locations, surface roughness, and other experimental features. However, as can be seen from Figs. 7 and 8, a single value of t^*_{sep} for each geometry worked well indicating that it is relatively insensitive to incidence. Empirically determined values of t^*_{sep} summarized in Table 1 for each geometry studied show a range of: $0.72 \leq t^*_{\text{sep}} \leq 1.0$. Note that setting t^*_{sep} sets θ^*_{sep} through the constraint $\theta^*_{\text{sep}} e^{\kappa_h t^*_{\text{sep}}} = 1$.

In the interests of applying the present model to other geometries where t^*_{sep} is not known a priori we make the following recommendations. For geometries with rounded noses and constant midbodies, such as the DRDC STR and DARPA SUBOFF, a reasonable estimate of t^*_{sep} is the value corresponding to the start of the midbody. This works reasonably well, because separation is inhibited by the rapid expansion of the nose at least until $\mathrm{d}a^*/\mathrm{d}\tau^*$ is sufficiently small that the second term in Eq. (4) is no longer significant. Evidence of this is given in Fig. 7, which shows that the CFD data agrees with the homogenous solution until the start of the tail for both the DRDC STR and DARPA SUBOFF geometries. For bodies with gradual spheroidal-shaped noses, such as the Series-58 Model 4621 and ellipsoids of varying slenderness, estimating an appropriate value for t^*_{sep} is more difficult, because separation will typically appear before the point of maximum thickness. Figure 9 illustrates the dependence of the separation-line model on t^*_{sep} in the case of the Series-58 Model 4621 at $\alpha = 12$ deg. Choosing $t^*_{\text{sep}} = 0.5$ results in overpredicting θ along much of the body, while choosing $t^*_{\text{sep}} = 1.25$ (the point of maximum thickness) results in underpredicting θ along much of the body. A mitigating factor to this uncertainty is that the influence of t^*_{sep} decays along the body so that the separation line along the tail reasonably well for each of these choices.

D. Limits of Applicability

The model developed here is applicable to fully turbulent flows with symmetric steady wakes. Its application is therefore restricted to high Reynolds numbers, $Re > 10^7$, and moderate angles of incidence and slenderness. Ericsson and Reding [2] surveyed the literature on high-incidence missile aerodynamics and concluded that leeside vortices become asymmetric at incidence angles between $\alpha = 25$ and 35 deg and unsteady at incidence angles between $\alpha = 60$ and 70 deg.

Table 1 Values of t^*_{sep} used to model separation lines shown in Figs. 7 and 8.

Geometry	t^*_{sep}	θ^*_{sep}
DRDC STR	1.0	0.607
Series-58 Model 4621	0.72	0.698
DARPA SUBOFF	0.75	0.687
6:1 Spheroid	1.0	0.607

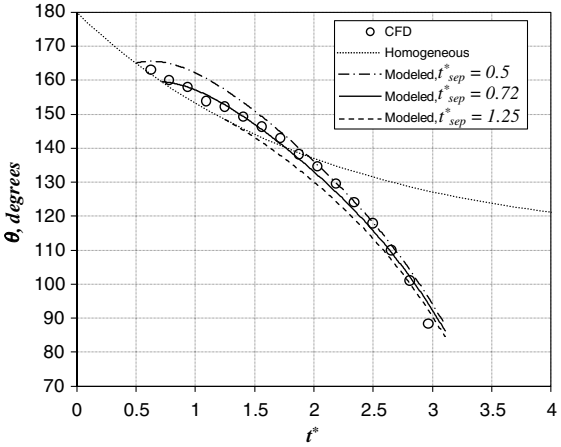

Fig. 9 Sensitivity of t^*_{sep} in Eq. (4) for the Series-58 Model 4621 geometry at $\alpha = 12$ deg.

They present the following empirical formula for determining the maximum angle of incidence for a steady symmetric wake: $\alpha \leq 8.4 a_{\max}/l$.

VI. Conclusions

A separation-line model for slender bodies of revolution with tapered tails in translation at moderate incidence and high Reynolds number was presented. The model is an extension of the previous work of Schindel [3] for missile-shaped bodies. It was found that the rate of windward movement of the separation line is dependent on the rate of change of the body radius. Modeled separation lines for four slender axisymmetric bodies with tapered tails are compared to CFD predictions and experimental measurement for incidence angles ranging from 6 to 30 deg and Reynolds numbers ranging from 4.2 to 23×10^6 with good agreement.

Acknowledgments

The authors would like to acknowledge that this work has been partially funded through the Natural Sciences and Engineering Research Council Discovery Grant of author A. G. L. Holloway. The authors would also like to acknowledge QinetiQ and the United Kingdom Ministry of Defence for their contribution to the Reynolds stress model Reynolds-averaged Navier–Stokes simulations on the Series-58 Model 4621, and the National Research Council Canada Institute for Aerospace Research for their contributions to Defence Research and Development Canada static-test-rig experiments.

References

[1] Allen, H. J., and Perkins, E. W., "Characteristics of Flow over Inclined Bodies of Revolution," NACA RM A50L07, March 1951.

[2] Ericsson, L. E., and Reding, J. P., "Vortex-Induced Asymmetric Loads in 2D and 3D Flows," AIAA 18th Aerospace Sciences Meeting, Pasadena, CA, AIAA Paper 1080-181, 14–16 Jan. 1980.

[3] Schindel, L. H., "Effects of Vortex Separation on the Lift Distribution on Bodies of Elliptic Cross Section," *Journal of Aircraft*, Vol. 6, No. 6, 1969, pp. 537–543. doi:10.2514/3.44102

[4] Lighthill, J. M., *Boundary Layer Theory, In Laminar Boundary Layers*, edited by L. Rosenhead, Oxford Univ. Press, Oxford, 1963, Chap. 2.

[5] Yates, L. A., and Chapman, G. T., "Streamlines, Vorticity Lines, and Vortices Around Three-Dimensional Bodies," *AIAA Journal*, Vol. 30, No. 7, 1992, pp. 1819–1826. doi:10.2514/3.11142.

[6] Simpson, R. L., "Aspects of Turbulent Boundary Layer Separation," *Progress in Aerospace Sciences*, Vol. 32, Nov. 1996, pp. 457–521. doi:10.1016/0376-0421(95)00012-7

[7] Wetzel, T. G., and Simpson, R. L., "Measurement of Three-Dimensional Crossflow Separation," *AIAA Journal*, Vol. 36, No. 4, 1998, pp. 557–564. doi:10.2514/2.429

[8] Ahn, S., and Simpson, R. L., "Crossflow Separation on a Prolate Spheroid at Angles of Attack," 30th Aerospace Sciences Meeting and Exhibit, AIAA Paper 92-0428, Jan. 1992.

[9] Chesnakas, C. J., and Simpson, R. L., "Detailed Investigation of the Three-Dimensional Separation About a 6:1 Prolate Spheroid," *AIAA Journal*, Vol. 35, No. 6, 1997, pp. 990–999. doi:10.2514/2.208

[10] Jeans, T. L., Watt, G. D., Gerber, A. G., Holloway, A. G. L., and Baker, C. R., "High Resolution Reynolds-Averaged Navier–Stokes Flow Predictions over Axisymmetric Bodies with Tapered Tails," *AIAA Journal*, Vol. 47, No. 1, 2009, pp. 19–32. doi:10.2514/1.30911

[11] Holloway, A. G. L., Gerber, A. G., Zhang, T. T., Maxwell, J. A., and Watt, G. D., "Simulation and Modeling of the Flow over Axisymmetric Submarine Hulls in Steady Turning," *28th Symposium on Naval Hydrodynamics*, Pasadena, CA, Sept. 2010.

[12] Watt, G. D., Nguyen, V. D., Cooper, K. R., and Tanguay, B., "Wind Tunnel Investigations of Submarine Hydrodynamics: The Development of the DREA Static Test Rig and Some Results," *Canadian Aeronautics and Space Journal*, Vol. 39, No. 3, 1993, pp. 119–126.

[13] Grover, N. C., Huang, T. T., and Chang, M. S., "Geometric Characteristics of DARPA SUBOFF Models (DTRC Models Nos. 5470 and 5471)," David Taylor Research Center, Ship Hydrodynamics Dept., Rept. 1298-01, Bethesda, MD, 1989.

[14] Van Randwijck, E. F., and Feldman, J. P., "Results of Experiments with a Segmented Model to Investigate the Distribution of the Hydrodynamic Forces and Moments on a Streamlined Body of Revolution at an Angle of Attack or with a Pitching Angular Velocity," Naval Surface Warfare Center, Carderock Div., Rept. NSWCCD-50-TR-2000/008, Bethesda, MD, Feb. 2000.

[15] Watt, G. D., Tanguay, B., and Cooper, K. R., "Submarine Hydrodynamics in the Wind Tunnel: The DREA Static Test Rig," *Warship '91: Royal Institution of Naval Architects International Symposium on Naval Submarines 3*, Royal Inst. of Naval Architects, London, May 1991.

[16] Nguyen, V. D., Drolet, Y., and Watt, G. D., "Interference of Various Support Strut Configurations in Wind Tunnel Tests on a Submarine Model," 33rd Aerospace Sciences Meeting and Exhibit, AIAA Paper 95-0443, Jan. 1995.

[17] Roddy, R. F., "Investigation of the Stability and Control Characteristics of Several Configurations of the DARPA SUBOFF Model from Captive Model Experiments," David Taylor Research Center, Ship Hydrodynamics Dept., Rept. 1298-08, Bethesda, MD, Sept. 1990.

[18] Baker, C. R., "A Strategic Meshing Approach to Modeling Hydrodynamic Flow Around Streamlined Axisymmetric Shapes," M.S. Thesis, Department of Mechanical Engineering, Univ. of New Brunswick, New Brunswick, Canada, March 2006.

[19] Watt, G. D., Baker, C. R., Gerber, A. G., and Fouts, C., "Scripted Hybrid Mesh Adaptation for High Incidence RANS Flows About Axisymmetric Shapes," 44th AIAA Aerospace Sciences Meeting and Exhibit, AIAA Paper 2006-886, Reno, NV, Jan. 2006.

[20] Zhang, J. T., "RANS Simulations of Axisymmetric Bodies in Turning," M.S. Thesis, Department of Mechanical Engineering, Univ. of New Brunswick, New Brunswick, Canada, April 2010.

[21] Launder, B. E., Reece, G. J., and Rodi, W., "Progress in the Developments of a Reynolds-Stress Turbulence Closure," *Journal of Fluid Mechanics*, Vol. 68, No. 3, April 1975, pp. 537–566. doi:10.1017/S0022112075001814

[22] Bryson, A. E., "Symmetric Vortex Separation on Circular Cylinders and Cones," *Journal of Applied Mechanics*, Vol. 26, 1959, pp. 643–648.

[23] Sarpkaya, T., "Separated Flow About Lifting Bodies and Impulsive Flow About Cylinders," *AIAA Journal*, Vol. 4, No. 3, 1966, pp. 414–420. doi:10.2514/3.3453

[24] Panton, R. L., *Incompressible Flow*, 2nd ed., Wiley, New York, 1996.